Title
Paleodust variability since the Last Glacial Maximum and implications for iron inputs to the ocean

Journal
Geophysical Research Letters, 43(8)

ISSN
0094-8276

Authors
Albani, S
Mahowald, NM
Murphy, LN
et al.

Publication Date
2016-04-28

DOI
10.1002/2016gl067911

AGU PUBLICATIONS

Geophysical Research Letters

RESEARCH LETTER
10.1002/2016GL067911

Key Points:
- Data-constrained time-slice CESM simulations estimate global dust variability since LGM
- Budgets and uncertainties in dust and soluble iron deposition to key ocean regions for biogeochemical cycles
- Elevated soluble iron inputs to the Atlantic sector of the Southern Ocean in the LGM

Supporting Information:
- Supporting Information S1

Correspondence to:
S. Albani,
s.albani@uni-koeln.de

Citation:
Albani, S., et al. (2016), Paleodust variability since the Last Glacial Maximum and implications for iron inputs to the ocean, *Geophys. Res. Lett.*, *43*, 3944–3954, doi:10.1002/2016GL067911.

Received 22 JAN 2016
Accepted 25 MAR 2016
Accepted article online 31 MAR 2016
Published online 28 APR 2016

Paleodust variability since the Last Glacial Maximum and implications for iron inputs to the ocean

S. Albani[1,2], N. M. Mahowald[1], L. N. Murphy[3], R. Raiswell[4], J. K. Moore[5], R. F. Anderson[6], D. McGee[7], L. I. Bradtmiller[8], B. Delmonte[9], P. P. Hesse[10], and P. A. Mayewski[11]

[1]Department of Earth and Atmospheric Sciences, Cornell University, Ithaca, New York, USA, [2]Now at the Institute for Geophysics and Meteorology, University of Cologne, Cologne, Germany, [3]Rosenstiel School of Marine and Atmospheric Science, University of Miami, Miami, Florida, USA, [4]School of Earth and Environment, Faculty of Environment, University of Leeds, Leeds, UK, [5]Department of Earth System Science, University of California, Irvine, California, USA, [6]Lamont-Doherty Earth Observatory and Department of Earth and Environmental Sciences, Columbia University, Palisades, New York, USA, [7]Department of Earth, Atmospheric and Planetary Sciences, Massachusetts Institute of Technology, Cambridge, Massachusetts, USA, [8]Department of Environmental Studies, Macalester College, Saint Paul, Minnesota, USA, [9]Department of Earth and Environmental Sciences, University of Milano-Bicocca, Milano, Italy, [10]Department of Environmental Sciences, Macquarie University, Sydney, New South Wales, Australia, [11]Climate Change Institute, University of Maine, Orono, Maine, USA

Abstract Changing climate conditions affect dust emissions and the global dust cycle, which in turn affects climate and biogeochemistry. In this study we use observationally constrained model reconstructions of the global dust cycle since the Last Glacial Maximum, combined with different simplified assumptions of atmospheric and sea ice processing of dust-borne iron, to provide estimates of soluble iron deposition to the oceans. For different climate conditions, we discuss uncertainties in model-based estimates of atmospheric processing and dust deposition to key oceanic regions, highlighting the large degree of uncertainty of this important variable for ocean biogeochemistry and the global carbon cycle. We also show the role of sea ice acting as a time buffer and processing agent, which results in a delayed and pulse-like soluble iron release into the ocean during the melting season, with monthly peaks up to ~17 Gg/month released into the Southern Oceans during the Last Glacial Maximum (LGM).

1. Introduction

Mineral dust is an important component of the climate system of the Earth [*Shao et al.*, 2011]. Dust emissions occur in response to surface erosion initiated by wind stress on the land surface in arid or semiarid areas with low vegetation cover [*Particorena and Bergametti*, 1995; *Prospero et al.*, 2002]. Fine-grained ($<10\,\mu m$ diameter) dust aerosols undergo long-range transport, with average lifetimes of a few days. Airborne dust particles impact cloud microphysics [*Boucher et al.*, 2013] and scatter and absorb solar and terrestrial radiation, altering the energy budget of the atmosphere [*Miller and Tegen*, 1998; *Balkanski et al.*, 2007]. Together with emission and transport, size-dependent dry and wet deposition scavenging processes shape the spatial features of the global dust cycle's mass balance, as well as the size distribution of dust particles [*Mahowald et al.*, 2014]. Dust acts as a carrier for elements (phosphorous and iron) that can limit the productivity in land [*Okin et al.*, 2004] and marine [*Martin et al.*, 1990; *Jickells et al.*, 2005; *Krishnamurthy et al.*, 2010; *Moore et al.*, 2013] ecosystems, modifying carbon sequestration.

The stratigraphic preservation of dust deposition in natural archives—such as ice cores, loess/paleosol sequences, or marine sediments—allows, under opportune circumstances, quantitative reconstructions of past Dust Mass Accumulation Rates (DMARs), which can be consistently used to constrain the global dust cycle [*Kohfeld and Harrison*, 2001; *Maher et al.*, 2010; *Albani et al.*, 2015].

We analyze the variability of the global dust cycle simulated with the Community Earth System Model (CESM) constrained by size-resolved observations of DMAR at different time slices between the Last Glacial Maximum (LGM) ~21,000 years before present (21 ka B.P.) up to the preindustrial (PI) climate, examining uncertainties in data model comparisons of dust deposition in key regions. We then estimate soluble iron (solFe) deposition using different sets of assumptions and calculate deposition budgets for different ocean regions. Finally, we discuss the role of seasonal sea ice in acting as a temporal buffer and leaching agent for solFe release into the oceans. The iron released from melting sea ice can impact phytoplankton community composition and bloom dynamics, productivity, and carbon export [*Abelmann et al.*, 2006, 2015; *Wang et al.*, 2014].

2. Methods

The CESM is a fully coupled global Earth System Model [*Gent et al*., 2011] that contributes to the Coupled Modelling Intercomparison Project (CMIP)/Paleoclimate Modelling Intercomparison Project (PMIP) [*Braconnot et al*., 2012; *Brady et al*., 2013]. The dust model [*Zender et al*., 2003; *Mahowald et al*., 2006] coupled to the CESM is based on a representation of the major components of dust cycle: mobilization, transport, and deposition. Modeled impacts on climate include direct radiative forcing, and radiative impacts of dust on both snow and sea ice [*Hunke and Lipscomb*, 2008; *Ganopolski et al*., 2010; *Bauer and Ganopolski*, 2014]. We use CESM version 1.0.5 with the state of the art version of the dust Bulk Aerosol Model (sectional model representing dust in four size bins spanning 0.1–10 μm diameter) coupled to the Community Atmosphere Model 4 [*Albani et al*., 2014] to simulate the global climate and the dust cycle during different periods, in climate equilibrium conditions.

Time resolution over the study period is achieved by performing new simulations complementary to detailed previous work [*Albani et al*., 2014, 2015; *Murphy et al*., 2014]. A total of eight simulations are included: PI (1850 A.D.), 2 ka B.P., 4 ka B.P., MH (6 ka B.P.), 8 ka B.P., 10 ka B.P., H1 (16 ka B.P.), and LGM (21 ka B.P.)—see Table S1 in the supporting information for details.

We used the PMIP3 equilibrium simulations as initial conditions, following the PMIP3 protocol for greenhouse gas concentrations, land and ice sheets, and the use of PI vegetation [*Brady et al*., 2013]. Dust emissions account for changes in vegetation area by scaling the erodible surface of each grid cell based on the fractional vegetation cover simulated with the BIOME4 model [*Kaplan et al*., 2003; *Albani et al*., 2014]. The magnitude and spatial features of dust emissions were constrained by particle size-resolved DMAR data for each climate scenario and provenance fingerprinting with dust radiogenic isotopes [*Albani et al*., 2014, 2015]. A new simulation for PI climate assumes that soil erodibilty is the same as for the late Holocene ~2 ka B.P., except we did not include glaciogenic sources in Alaska or dune mobilization in Nebraska [*Albani et al*., 2015]. The simulation for a Heinrich stadial [*Murphy et al*., 2014] was associated with H1 (~16 ka B.P.) and rerun with a reduced soil erodibility scale factor for South America (one fourth of LGM, based on EPICA Dome C data) to account for the shrinking of glaciogenic sources compared to the LGM [e.g., *Lambert et al*., 2008]. Current limitations of our approach include the use of time slices rather than a transient simulation, the lack of a dynamical vegetation model, and several assumptions concerning the homogeneous dust elemental composition and the processing of dust-borne iron, including paleofires.

The bioavailable fraction of iron is not well known, partly because of differences in analytical procedures [*Mahowald et al*., 2009; *Baker and Croot*, 2010]. Observational evidence indicates (a) atmospheric processing of iron to soluble iron [*Zhu et al*., 1997; *Meskhidze et al*., 2005], (b) varying solubility under different dust and aerosol chemical conditions [*Journet et al*., 2008; *Shi et al*., 2012; *Sholkovitz et al*., 2012], and (c) direct emission of soluble iron from combustion sources [*Guieu et al*., 2005; *Chuang et al*., 2005; *Luo et al*., 2008]. We assume 3.5% (mass) iron content in dust [*Watson et al*., 2000] and that the labile iron is soluble [*Jickells and Spokes*, 2001]. We estimate solFe deposition to the ocean with five different sets of assumptions (for details, see supporting information Figure S5), in order to constrain the uncertainties in atmospheric processing based on published hypotheses. The five scenarios include one case assuming constant iron solubility of 2% (CON) [e.g., *Moore et al*., 2006; *Tagliabue et al*., 2009], as well as four different scenarios which also consider emissions of iron from PI biomass burning [*Luo et al*., 2008]. CON2 is simply the combination of CON and PI biomass burning iron. MOD (based on *Luo et al*. [2008] and *Mahowald et al*. [2009]), SIZ, and INV (based on *Sholkovitz et al*. [2012]) consider processing of dust-borne iron and biomass burning emissions (Figure S5). In addition, we estimate (a) the uncertainties related to dust deposition and (b) the potential role of dust processing by sea ice, which observations suggest increases iron solubility by a factor of ~2.5 [*Raiswell et al*., 2016].

3. Results and Discussion

3.1. Mass Balance of the Global Dust Cycle Since the LGM

CESM reconstructions estimate higher global emissions during the late glacial stages than during the Holocene, with a minimum in the early/mid-Holocene (Figures 1a–1d and supporting information Figure S1), in line with observations of DMAR [*Kohfeld and Harrison*, 2001; *Maher et al*., 2010]. The LGM was

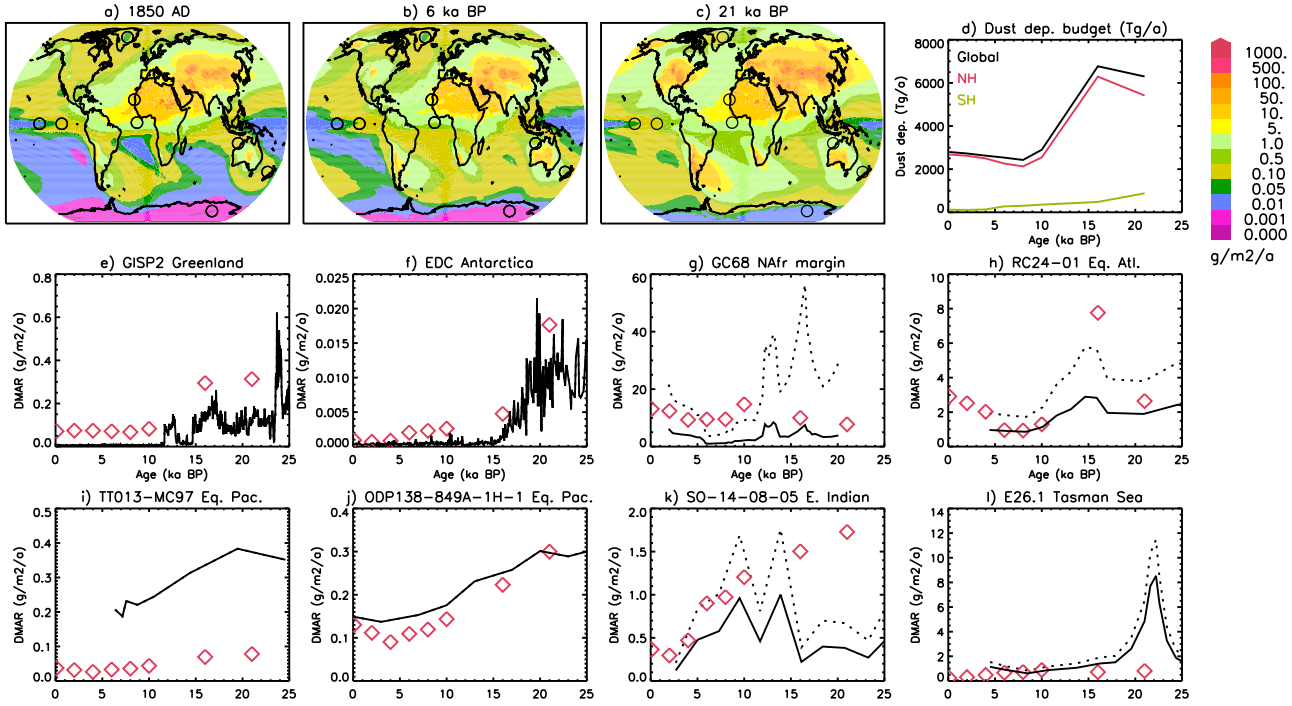

Figure 1. (a–c) Time series of dust deposition (0.1–10 μm) in the CESM simulations for PI, MH, and LGM climates. (d) Mass budgets of dust deposition (global, NH, and SH). (e–l) Model (red diamonds) deposition compared to DMAR observations (solid line: fine (<10 μm); dotted: bulk).

characterized by high dust deposition rates in both hemispheres (Figure 1c) [*Albani et al.* 2014]. H1 coincides with larger emissions from the Northern Hemisphere (NH), resulting in enhanced dust deposition globally at 16 ka B.P. (6771 Tg/a) compared to 21 ka B.P. (6294 Tg/a), despite the drastic reduction of glaciogenic dust emissions from South America and in the Southern Hemisphere (SH) [*Lambert et al.*, 2008; *Martínez-García et al.*, 2009] (Figure 1d). By the early Holocene, global dust emissions had reduced significantly to ~2900 Tg/a at 10 ka B.P., shrinking to a minimum (2427 Tg/a) ~8 ka B.P. and later expanding again until PI (~2798 Tg/a). Concurrently, the emissions from the SH decreased during the Holocene, while the NH emissions were increasing, consistent with the insolation-induced changes in seasonality and the monsoon systems [*Braconnot et al.*, 2007]. At the same time emissions were also shifting gradually from Asia toward North Africa in terms of mass balance [*Albani et al.*, 2015] (Figures 1a–1c).

For reference, global dust emission (and deposition) in previous studies ranged from ~1000 to ~5000 Tg/a for interglacial climates and from ~2000 to ~14,000 Tg/a for the LGM [e.g., *Werner et al.*, 2002; *Lunt and Valdes*, 2002; *Claquin et al.*, 2003; *Mahowald et al.*, 2006; *Takemura et al.*, 2009; *Bauer and Ganopolski*, 2010, 2014; *Yue et al.*, 2011; *Sudarchikova et al.*, 2015]. For the present day, the AeroCom median of 15 global models is 1257 Tg/a [*Huneeus et al.*, 2011]. Note that the potential for long-range transport, more relevant for deposition to the oceans, is highly dependent on modeled particle size distributions [*Albani et al.*, 2014; *Mahowald et al.*, 2014]. Here we estimate that 440 and 826 Tg/a dust are deposited to the world's oceans in PI and LGM, respectively (Table S1). For current climate conditions, a composite estimate of dust deposition to the ocean from different models amounts to 450 Tg/a [*Jickells et al.*, 2005].

Our simulations capture the trends in observed dust deposition in Greenland (Figure 1e) and Antarctica (Figure 1f), but not all the details, because the model was constrained with a larger data set [*Albani et al.*, 2014, 2015]. The simulated LGM/Holocene dust deposition ratio is ~4 for GISP2, compared to ~17 from the observations (average 19–23 ka BP) for the LGM [*Mayewski et al.*, 1997], which may be substantially influenced by changes in atmospheric circulation [*Serno et al.*, 2015] that are not captured by the model. At Dome C, the simulated LGM/Holocene ratio is larger (~10) but still less than the observations (~25) [*Delmonte et al.*, 2004]. The absolute values of deposition fluxes are overestimated for the Holocene (LGM) by a factor of ~10 (3) in Greenland and ~4 (20) in Antarctica. Part of this overestimation is probably related to the model's relatively too smooth gradient in dust deposition between sources and remote regions [*Albani et al.*, 2014; *Mahowald et al.*, 2014].

The CESM-based dust deposition at sites downwind from North Africa captures features of the observed DMAR (note the distinction between fine fraction and bulk in Figure 1), including the increase in dust deposition during H1 compared to the LGM, and the early/mid-Holocene dust minimum (Figures 1g and 1h). DMAR (fine) is better reproduced in the equatorial Atlantic (Figure 1h) than in the North African margin, where it is overestimated by the model (Figure 1g), possibly because of inaccurate representation of the temporal dynamics of dust source activation or wind patterns, or an overestimation of wet deposition of dust in the CESM [*Albani et al*., 2015; *Scanza et al*., 2015]. Alternatively, the observed DMAR at GC68 may be underestimated, as it is comparable in magnitude to remote sites in the equatorial Pacific in the early to mid-Holocene [*Albani et al*., 2015]. For GC68 the partitioning of riverine versus eolian contributions is based on end-member decomposition of the grain size distribution [*McGee et al*., 2013]. This approach has its greatest uncertainties in the fine fraction. On the other hand, DMAR estimates from equatorial Atlantic core RC24-01 also have large uncertainties due to its relatively coarse age model and lower sediment accumulation rates with larger impacts of bioturbation. Down-core measurements of particle size distributions were not performed for RC24-01 [*Bradtmiller et al*., 2007] but were approximated by a constant fraction (0.5) of particles $< 10\,\mu m$, based on nearby sediment trap measurements [*Ratmeyer et al*., 1999]. Therefore, part of the model-observation mismatch may be related to uncertainties in estimating the fine fraction of the total eolian flux (Figures 1g and 1h, dotted line versus solid line), suggesting possible inconsistency among observations themselves [*Albani et al*., 2015].

In the equatorial Pacific our reconstructions agree with the magnitude and trends of dust deposition at 110° W but underestimate DMAR farther west at 140°W (Figures 1i and 1j) in both glacial and interglacial conditions. In our simulations, this seems at least in part related to the penetration of the North African dust plume across the Atlantic and into the Pacific, which may not be fully consistent with the latest observational evidence on dust provenance in the region (see also supporting information Figure S2). Another feature emerging from the observations is the N-S gradient in dust deposition, which remains relatively constant across the LGM-Holocene transition [*Anderson et al*., 2006; *McGee et al*., 2007]. This feature is partially reproduced by our simulations, but a minimum in simulated dust deposition at the equator is not found in the observations (Figure S2 and associated discussion in the supporting information). Biases in model precipitation evident for current climate could explain the mismatch (supporting information Figure S2); in our simulations the dust deposition flux, there is controlled primarily by the dust load (i.e., availability of dust) and modulated by the precipitation, as wet deposition is the dominant process for dust removal from the atmosphere (supporting information Figure S3). The "double ITCZ" is a known bias in the state of the art climate models [*Li and Xie*, 2014], and it may also account for very low dust deposition in the Western Pacific in the CESM [*Winckler et al*., 2008; *Albani et al*., 2014, 2015].

Our simulations reproduce the magnitude and trends of dust deposition at sites sampling the main Australian dust corridors [*Fitzsimmons et al*., 2013] during the Holocene but fail to capture late glacial trends. Too high dust deposition is simulated for the NW site (Figure 1k), whose trends [*Hesse and McTainsh*, 2003] are confirmed by a dust proxy from a nearby core [*Kuhnt et al*., 2015], whereas the LGM spike in dust deposition in the Tasman Sea record [*Hesse*, 1994] is not matched (Figure 1l). Simulated LGM dust emissions are intense both from the Lake Eyre Basin and the West, whereas only the former is a significant dust source in the PI (supporting information Figure S4). Paleoclimate and geomorphological evidence is consistent with spatial variability in landscape response to LGM/deglacial climate oscillations, possibly related to the interplay between the monsoon and the Southern westerlies [*Fitzsimmons et al*., 2013]. On the other hand, the CESM shows no significant variability in the ITCZ on glacial-interglacial time scales [*Brady et al*., 2013]. Our simulations underestimate dust deposition at site PS75/59-2 (125°W, 54°S) [*Lamy et al*., 2014] by an order of magnitude, although they capture the observational LGM/Holocene ratio (~3) (supporting information Figure S1).

Interestingly, observed Holocene DMAR at PS75/59-2 are lower than the upwind Tasman Sea record, but of the same magnitude as the NW site (fine fraction), which is very close to the continent. Similarly, *Albani et al*. [2015] pointed out that Holocene DMARs in the South Atlantic [*Anderson et al*., 2014; *Martínez-García et al*., 2009] are comparable to those form the North Atlantic (fine fraction), in a region where satellites show little dust today [*Prospero et al*., 2002], suggesting possible incongruences as discussed earlier for the North Atlantic. More data of both DMAR and particle size distribution are needed to constrain the models and tackle this problem.

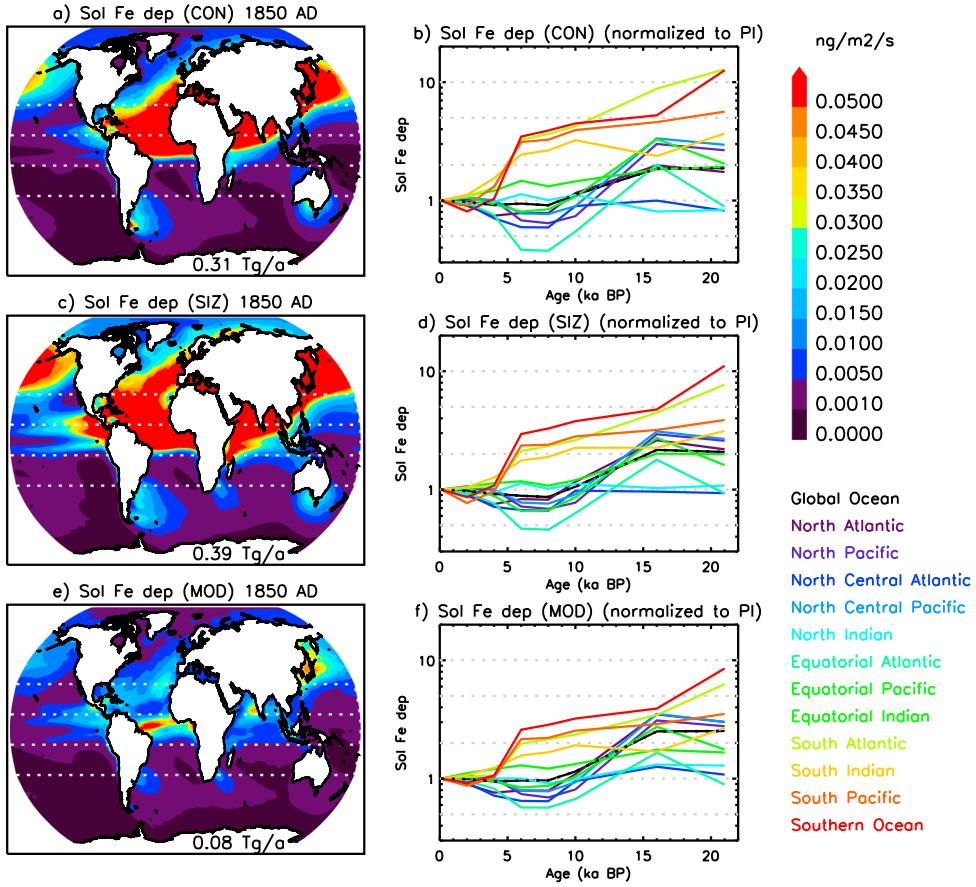

Figure 2. (a, c, and e) Simulated solFe deposition flux (ng/m^2/s) to the oceans, including on sea ice, during the PI using different sets of assumptions. Printed numbers indicate the global deposition to the ocean and sea ice. White lines indicate the limits of ocean regions [*Gregg et al*., 2003]. (b, d, and f) Normalized time series (to PI) of simulated solFe deposition to different ocean regions, for the corresponding cases.

3.2. Soluble Iron Inputs to the Oceans

A common assumption that dust-borne iron has a constant solubility of 2% (CON) [e.g., *Tagliabue et al*., 2009] (Figure 2a) hides the spatial variability that both dust composition [*Schroth et al*., 2009; *Journet et al*., 2013] and atmospheric processing [*Baker and Croot*, 2010; *Shi et al*., 2012] impart on bioavailable iron [*Jickells and Spokes*, 2001; *Mahowald et al*., 2009]. A sensitivity study including biomass burning sources of iron (CON2) is contrasted with other (MOD, SIZ, and INV) simplified approximations of atmospheric dust processing and sensitivity to aerosol abundance (supporting information Figure S5) and suggests a different regional distribution of deposition.

There are also significant differences in the global estimates of solFe deposition to the ocean, ranging from 0.08 to 0.39 Tg/a for PI (Figures 2a, 2c, and 2e and supporting information Figure S5) and 0.20 to 0.82 for the LGM, with MOD and SIZ giving the smaller and larger estimates, respectively. All cases show larger temporal variability (absolute and relative) in the Southern Ocean and North Pacific regions (Figures 2b, 2d, 2f, and 2h; supporting information Figure S5; and supporting information Tables S2–S6), in line with observed changes in dust deposition of a factor of ~5 [e.g., *Martínez-García et al*., 2009; *Serno et al*., 2015].

For CON, we estimate how uncertainties in dust deposition (without specifically analyzing the large range of estimates using different observational approaches, which is beyond the scope of this paper) propagate into solFe deposition budgets for key oceanic regions, based on the model-observation comparison (Figure 3). Note that in general, we expect model and observations comparisons of dust deposition to be scattered within 1 order of magnitude [*Mahowald et al*., 2011; *Albani et al*., 2014]. CESM simulations tuned with global data sets [*Albani et al*., 2014, 2015] are on the high end for deposition downwind of the North African plume

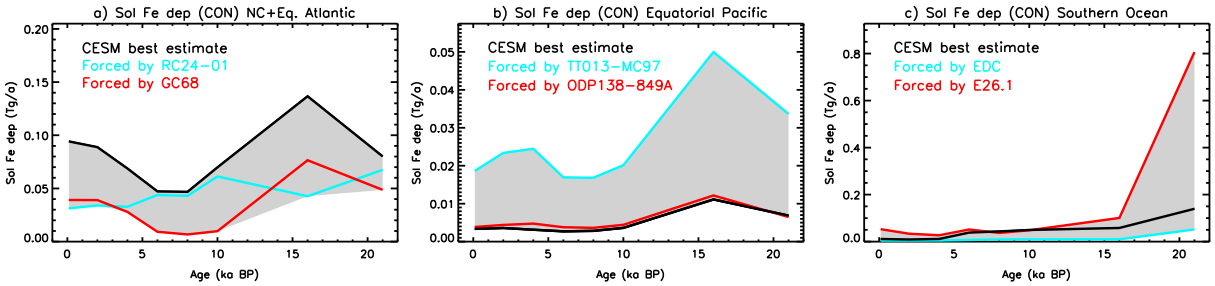

Figure 3. Time series of SolFe (CON) regional deposition rates (Tg/a) into oceanic regions, as in Figure 2: (a) North/Central + equatorial Atlantic, (b) equatorial Pacific, and (c) Southern Ocean. Black lines: CESM simulations. Colored lines: deposition rates scaled at each time based on the model-observation bias, i.e., dividing the CESM simulated value by the CESM simulation/observation ratio for each observational time series (observations averaged over 2 ka periods). Grey shading: uncertainty envelope.

in the Atlantic, but on the low end in the equatorial Pacific, possibly suggesting an overall too sharp reduction of the North African plume as it moves westward, or a different source mix in the model, with possible underestimation of South and central American sources (Figures 3a and 3b and supporting information Figure S2). For the southern oceans (>30°S) significant uncertainties arise depending on the specific choice of observational constraints (Figure 3c), highlighting the importance of gathering more observations of deposition magnitude. Note that uncertainties related to the gradient in mid-to-high latitudes dust depositions discussed in section 3.1 may contribute to the overall uncertainty in estimates of dust/iron deposition to the Southern Ocean.

The sea ice component of CESM [*Jahn et al.*, 2012; *Wang et al.*, 2014] allows partitioning of dust deposition onto open waters compared to sea ice. In the high-latitude oceans the fraction of dust (and associated iron) that is deposited on sea ice increases closer to the poles (Figures 4a and 4b). At latitudes > 45°S in the Southern Ocean dust-borne iron intercepted by sea ice (blue, dotted line in Figures 4c, 4d, 4g, and 4h) in our PI simulations represents about one eighth of the deposition over the open ocean, but the proportions become comparable during LGM, because of an increase in sea ice extent and a preferential strengthening of sources supplying dust to regions with high sea ice cover. A similar situation is simulated in the Arctic (Figures 4c, 4d, 4g, and 4h).

The climatological annual cycle of iron inputs into the oceans shows a marked seasonality, determined by the interplay between direct atmospheric inputs into the ocean and the inputs mediated by the sea ice. Sea ice itself represents a weathering environment [*Edwards and Sedwick*, 2001; *Lannuzel et al.*, 2007; *Abelmann et al.*, 2015], where iron solubility was shown to potentially increase by a factor of ~2.5 ± 2.5 as a result of photoreductive processes in ice and melting/freezing cycles which allow intermittent chemical weathering to form Fe as (oxyhydr)oxides [*Raiswell et al.*, 2016]. Dust deposition on sea ice results in a delayed and pulse-like solFe release into the ocean as sea ice melts annually (Figures 4c, 4d, 4g, and 4h). This pulse of iron comes just at the beginning of the growing season and may favor the larger phytoplankton and bloom development, which leads to more efficient export of carbon to the ocean interior [*Wang et al.*, 2014].

The simulated net solFe input into the high-latitude oceans during the peak months is 3 times higher in the NH than the SH (Figure 4). The spatial features of iron deposition show that certain regions such as the Atlantic Sector receive substantially more iron than the average Southern Ocean (Figures 4a and 4b). During the LGM, the magnitude and relative importance of sea ice mediated release of solFe into the ocean becomes even larger (Figures 4g and 4h).

We estimate (CON scenario) that up to 6 and 90 Gg/a solFe could be released into the Southern Ocean south of 45°S (33 and 88 in the NH high-latitude oceans) for PI climate conditions and the LGM, respectively (Figure 4). In the LGM/PI comparison, sea ice processing amplifies solFe input to the ocean by 10% in the NH and 22% in the SH on average. Additional processes supply iron in the real ocean [e.g., *Kohfeld et al.*, 2005; *Lambert et al.*, 2015], including hydrothermal vents [*Tagliabue et al.*, 2014], shelf sediments [*Lam and Bishop*, 2008; *Moore and Braucher*, 2008], and ice rafted debris [*Kohfeld and Harrison*, 2001; *Raiswell et al.*, 2016].

Overall, our study shows that substantial uncertainty exists in current estimates of solFe deposition to the ocean, when accounting for the combined uncertainties from dust deposition, atmospheric processing,

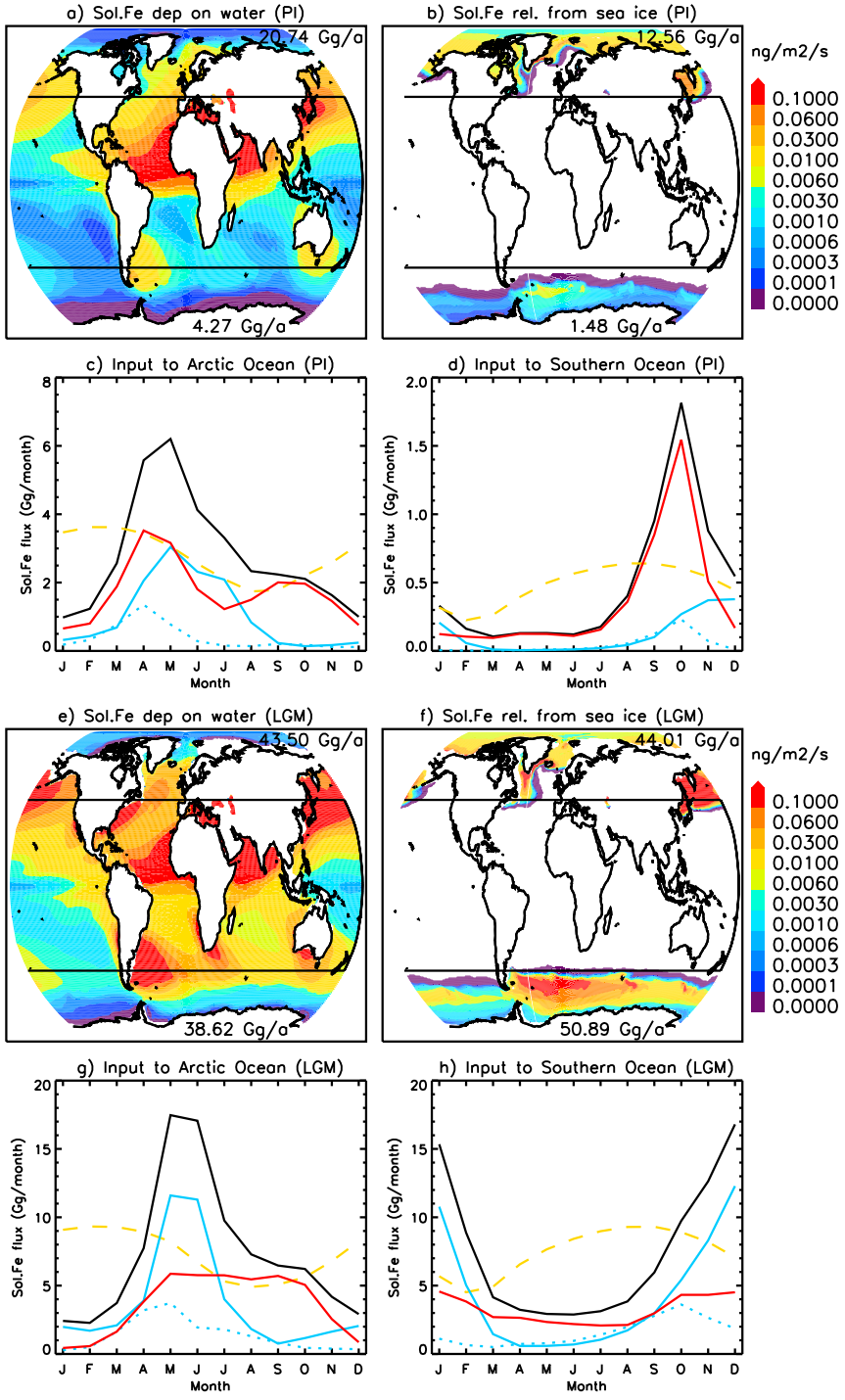

Figure 4. Simulated solFe (CON) fluxes (ng/m^2/s) from the atmosphere to the ocean open waters and from sea ice to the ocean for (a, b) PI and (e, f) LGM climate. Printed numbers indicate the total solFe fluxes to the ocean in the high-latitude (>45°N/S) regions (black lines). (c, d, g, and h) The average annual cycle (Gg/month) of simulated solFe input to the ocean (black), partitioned into direct atmospheric input (red), and released after processing from sea ice (blue, solid), as well as atmospheric solFe input to the sea ice (blue, dotted). Sea ice extent (yellow) over the same high-latitude regions is scaled independently for plotting purposes.

and sea ice processing (supporting information Figure S6). In the most extreme scenario ~1.6 Tg/a solFe could enter the ocean waters south of 30°S during the LGM.

4. Summary

For the first time, we provide data-constrained global model reconstructions of dust and solFe deposition at different time slices from the LGM to PI climate, complemented by a set of sensitivity studies designed to estimate the range of the composite uncertainty arising from uncertainties in dust deposition, atmospheric, and sea ice processing in regions of particular importance for ocean biogeochemistry and the carbon cycle.

The model reconstructions show a reasonably good agreement with observations of dust deposition from paleodust archives, both in terms of trends and absolute values [see *Albani et al*., 2015]. Global dust deposition reached a maximum during H1 ~ 16 ka B.P. (6771 Tg/a) and a minimum during the early/mid-Holocene ~8 ka B.P. (2427 Tg/a).

Estimates of dust-borne solFe deposition to the oceans using five different sets of assumptions reveal a wide uncertainty, with global estimates between 0.08 and 0.39 Tg/a for the PI climate and between 0.20 and 0.82 Tg/a for the LGM (CON scenario). The larger variations in LGM versus PI climate were simulated for the Southern Ocean and Northern Pacific, both regions where ocean biogeochemistry is sensitive to iron inputs [*Moore et al*., 2006; *Krishnamurthy et al*., 2010]. Our approach here uses several common methods for estimating soluble iron to examine the sensitivity of our results to assumptions [*Moore et al*., 2006; *Tagliabue et al*., 2009; *Luo et al*., 2008; *Sholkovitz et al*., 2012] and shows that combustion iron from paleofires could be important for paleoclimate simulations [*Ward et al*., 2012]. The details of the assumptions about iron solubility matter greatly for spatial and temporal variabilities in solFe deposition. Because evidence suggests that both the amount and the mineralogy of dust matters for solubility [*Schroth et al*., 2009; *Shi et al*., 2012], more data about the composition and/or sources of dust [*Grousset and Biscaye*, 2005] and other iron sources should be acquired.

Sea ice acts as a time buffer resulting in a delayed, pulsed solFe release into the ocean during the melting season, with peaks up to ~17 Gg/month released into the Southern Ocean during the LGM, if also considering the potential role of sea ice in iron processing (CON). The spatial features of solFe release into the ocean waters reveal comparable deposition rates in the Atlantic sector of the Southern Ocean and in low-latitude regions of moderately high dust flux, like the Caribbean, during the LGM.

A much larger range of estimates of solFe input to specific oceanic regions arises when considering the composite uncertainty of dust deposition, atmospheric, and sea ice processing.

Given the importance of the episodic nature of atmospheric inputs for ocean biogeochemistry [*Krishnamurthy et al*., 2010; *Guieu et al*., 2014], our results may prove valuable for testing the iron hypothesis, in line with observations supporting the idea that dust was a significant contributor to stimulating the glacial biological pump [*Ziegler et al*., 2013; *Lamy et al*., 2014; *Martínez-García et al*., 2014]. Further studies with coupled models simulating marine ecosystem dynamics are needed to determine the net export production, hence the net dust-induced effect on atmospheric CO_2 concentrations [*Falkowski et al*., 1998; *Moore et al*., 2006].

Acknowledgments
We acknowledge assistance from NSF grants 661541, 0932946, 1003509, and DOE-SC00006735. Computing resources were provided by the Climate Simulation Laboratory at NCAR's Computational and Information Systems Laboratory (CISL), sponsored by the National Science Foundation and other agencies. We appreciate support from the NCAR Paleoclimate Working Group. We thank David Bailey for his support in analyzing the CICE data. We would like to thank Amy Clement for discussions. Constructive comments from Eva Bauer and one anonymous reviewer were helpful for improving the manuscript. Data of soluble iron deposition in the different ocean basins are reported in the supporting information. Observational dust data and the CESM-based reconstructions of dust deposition fields are available upon request with the corresponding author. This is a contribution to the PAst Global changES (PAGES) working group on Dust Impact on Climate and Environment (DICE).

References

Abelmann, A., R. Gersonde, G. Cortese, G. Kuhn, and V. Smetacek (2006), Extensive phytoplankton blooms in the Atlantic sector of the glacial Southern Ocean, *Paleoceanography*, *21*, PA1013, doi:10.1029/2005PA001199.

Abelmann, A., et al. (2015), The seasonal sea-ice zone in the glacial Southern Ocean as a carbon sink, *Nat. Commun.*, *6*, 8136, doi:10.1038/ncomms9136.

Albani, S., N. M. Mahowald, A. T. Perry, R. A. Scanza, N. G. Heavens, C. S. Zender, V. Maggi, J. F. Kok, and B. L. Otto-Bliesner (2014), Improved dust representation in the Community Atmosphere Model, *J. Adv. Model. Earth Syst.*, *6*, 541–570, doi:10.1002/2013MS000279.

Albani, S., et al. (2015), Twelve thousand years of dust: The Holocene global dust cycle constrained by natural archives, *Clim. Past*, *11*, 869–903, doi:10.5194/cp-11-869-2015.

Anderson, R. F., M. Q. Fleisher, and Y. Lao (2006), Glacial–interglacial variability in the delivery of dust to the central equatorial Pacific Ocean, *Earth Planet. Sci. Lett.*, *242*, 406–414, doi:10.1016/j.epsl.2005.11.061.

Anderson, R. F., S. Barker, M. Fleisher, R. Gersonde, S. L. Goldstein, G. Kuhn, P. G. Mortyn, K. Pahnke, and J. P. Sachs (2014), Biological response to millennial variability of dust and nutrient supply in the Subantarctic South Atlantic Ocean, *Philos. Trans. A. Math. Phys. Eng. Sci.*, *372*, doi:10.1098/rsta.2013.0054.

Baker, A., and P. Croot (2010), Atmospheric and marine controls on aerosol iron solubility in seawater, *Mar. Chem.*, *120*, 4–13, doi:10.1016/j.marchem.2008.09.003.
Balkanski, Y., M. Schultz, T. Claquin, and S. Guibert (2007), Reevaluation of mineral aerosol radiative forcings suggests a better agreement with satellite and AERONET data, *Atmos. Chem. Phys.*, *7*, 81–95, doi:10.5194/acp-7-81-2007.
Bauer, E., and A. Ganopolski (2010), Aeolian dust modelling over the past four glacial cycles with CLIMBER-2, *Global Planet. Change*, *74*, 49–60, doi:10.1016/j.gloplacha.2010.07.009.
Bauer, E., and A. Ganopolski (2014), Sensitivity simulations with direct shortwave radiative forcing by aeolian dust during glacial cycles, *Clim. Past*, *10*(4), 1333–1348, doi:10.5194/cp-10-1333-2014.
Boucher, O., et al. (2013), Clouds and aerosols, in *Climate Change 2013: The Physical Science Basis. Contribution of Working Group I to the Fifth Assessment Report of the Intergovernmental Panel on Climate Change*, edited by T. F. Stocker et al., Cambridge Univ. Press, Cambridge, U. K., and New York.
Braconnot, P., et al. (2007), Results of PMIP2 coupled simulations of the mid-Holocene and Last Glacial Maximum—Part 1: Experiments and large-scale features, *Clim. Past*, *3*, 261–277, doi:10.5194/cp-3-261-2007.
Braconnot, P., S. P. Harrison, M. Kageyama, P. J. Bartlein, V. Masson-Delmotte, A. Abe-Ouchi, B. Otto-Bliesner, and Y. Zhao (2012), Evaluation of climate models using paleoclimatic data, *Nat. Clim. Change*, *2*, 417–424, doi:10.1038/nclimate1456.
Bradtmiller, L. I., R. F. Anderson, M. Q. Fleisher, and L. H. Burckle (2007), Opal burial in the equatorial Atlantic Ocean over the last 30 ka: Implications for glacial-interglacial changes in the ocean silicon cycle, *Paleoceanography*, *22*, PA4216, doi:10.1029/2007PA001443.
Brady, E. C., B. L. Otto-Bliesner, J. E. Kay, and N. Rosenbloom (2013), Sensitivity to glacial forcing in the CCSM4, *J. Clim.*, *26*, 1901–1925, doi:10.1175/JCLI-D-11-00416.1.
Chuang, P., R. Duvall, M. Shafer, and J. Schauer (2005), The origin of water-soluble particulate iron in the Asian atmospheric outflow, *Geophys. Res. Lett.*, *32*, L07813, doi:10.1029/2004GL021946.
Claquin, T., et al. (2003), Radiative forcing of climate by ice-age atmospheric dust, *Clim. Dyn.*, *20*, 193–202, doi:10.1007/s00382-002-0269-1.
Delmonte, B., J.-R. Petit, K. K. Andersen, I. Basile-Doelsch, V. Maggi, and V. Y. Lipenkov (2004), Dust size evidence for opposite regional atmospheric circulation changes over east Antarctica during the last climatic transition, *Clim. Dyn.*, *23*, 427–438, doi:10.1007/s00382-004-0450-9.
Edwards, R., and P. Sedwick (2001), Iron in East Antarctic snow: Implications for atmospheric iron deposition and algal production in Antarctic waters, *Geophys. Res. Lett.*, *28*(20), 3907–3910, doi:10.1029/2001GL012867.
Falkowski, P. G., R. T. Barber, and V. Smetacek (1998), Biogeochemical controls and feedbacks on ocean primary production, *Science*, *281*, 200–206, doi:10.1126/science.281.5374.200.
Fitzsimmons, K. E., et al. (2013), Late Quaternary palaeoenvironmental change in the Australian drylands, *Quat. Sci. Rev.*, *74*, 78–96, doi:10.1016/j.quascirev.2012.09.007.
Ganopolski, A., R. Calov, and M. Claussen (2010), Simulation of the last glacial cycle with a coupled climate ice-sheet model of intermediate complexity, *Clim. Past*, *6*, 229–244, doi:10.5194/cp-6-229-2010.
Gent, P. R., et al. (2011), The Community Climate System Model, version 4, *J. Clim.*, *24*(19), 4973–4991, doi:10.1175/2011JCLI4083.1.
Gregg, W. W., M. E. Conkright, P. Ginoux, J. E. O'Reilly, and N. W. Casey (2003), Ocean primary production and climate: Global decadal changes, *Geophys. Res. Lett.*, *30*(15), 1809, doi:10.1029/2003GL016889.
Grousset, F., and P. E. Biscaye (2005), Tracing dust sources and transport patterns using Sr, Nd and Pb isotopes, *Chem. Geol.*, *222*, 149–167, doi:10.1016/j.chemgeo.2005.05.006.
Guieu, C., S. Bonnet, T. Wagener, and M.-D. Loye-Pilot (2005), Biomass burning as a source of dissolved iron to the open ocean?, *Geophys. Res. Lett.*, *22*, L19608, doi:10.1029/2005GL022962.
Guieu, C., et al. (2014), The significance of the episodic nature of atmospheric deposition to Low Nutrient Low Chlorophyll regions, *Global Biogeochem. Cycles*, *28*, 1179–1198, doi:10.1002/2014GB004852.
Hesse, P. P. (1994), The record of continental dust from Australia in Tasman sea sediments, *Quat. Sci. Rev.*, *13*, 257–272, doi:10.1016/0277-3791(94)90029-9.
Hesse, P. P., and G. H. McTainsh (2003), Australian dust deposits: Modern processes and the Quaternary record, *Quat. Sci. Rev.*, *22*, 2007–2035, doi:10.1016/S0277-3791(03)00164-1.
Hunke, E. C., and W. H. Lipscomb (2008), CICE: The Los Alamos sea ice model, documentation and software, version 4.0. Los Alamos National Laboratory Tech. Rep. LA-CC-06-012, 76 pp.
Huneeus, N., et al. (2011), Global dust model intercomparison in AeroCom phase I, *Atmos. Chem. Phys.*, *11*, 7781–7816, doi:10.5194/acp-11-7781-2011.
Jahn, A., et al. (2012), Late 20th century simulation of Arctic sea ice and ocean properties in the CCSM4, *J. Clim.*, *25*(5), 1431–1452, doi:10.1175/JCLI-D-11-00201.1.
Jickells, T. D., and L. J. Spokes (2001), Atmospheric inputs to the ocean, in *The Biogeochemistry of Iron in Seawater*, edited by D. R. Turner and K. A. Huneter, pp. 123–251, Wiley, New York.
Jickells, T. D., et al. (2005), Global iron connections between desert dust, ocean biogeochemistry, and climate, *Science*, *308*, 67–71, doi:10.1126/science.1105959.
Journet, E., K. V. Desboeufs, S. Caquineau, and J.-L. Colin (2008), Mineralogy as a critical factor of dust iron solubility, *Geophys. Res. Lett.*, *35*, L07805, doi:10.1029/2007GL031589.
Journet, E., Y. Balkanski, and S. P. Harrison (2013), A new data set of soil mineralogy for dust-cycle modeling, *Atmos. Chem. Phys.*, *14*, 3801–3816, doi:10.5194/acp-14-3801-2014.
Kaplan, J. O., et al. (2003), Climate change and Arctic ecosystems: 2. Modeling, paleodata-model comparisons, and future projections, *J. Geophys. Res.*, *108*(D19), 8171, doi:10.1029/2002JD002559.
Kohfeld, K. E., and S. P. Harrison (2001), DIRTMAP: The geological record of dust, *Earth Sci. Rev.*, *54*, 81–114, doi:10.1016/S0012-8252(01)00042-3.
Kohfeld, K. E., C. Le Quéré, S. P. Harrison, and R. F. Anderson (2005), Role of marine biology in glacial-interglacial CO_2 cycles, *Science*, *308*, 74–78, doi:10.1126/science.1105375.
Krishnamurthy, A., J. K. Moore, N. Mahowald, C. Luo, and C. S. Zender (2010), Impacts of atmospheric nutrient inputs on marine biogeochemistry, *J. Geophys. Res.*, *115*, G01006, doi:10.1029/2009JG001115.
Kuhnt, W., A. Holbourn, J. Xu, B. Opdyke, P. De Deckker, U. Röhl, and M. Mudelsee (2015), Southern Hemisphere control on Australian monsoon variability during the late deglaciation and Holocene, *Nat. Commun.*, *6*, 5916, doi:10.1038/ncomms6916.
Lam, P., and J. Bishop (2008), The continental margin is a key source of iron to the North Pacific Ocean, *Geophys. Res. Lett.*, *35*, L07608, doi:10.1029/2008GL033294.

Lambert, F., B. Delmonte, J.-R. Petit, M. Bigler, P. R. Kaufmann, M. A. Hutterli, T. F. Stocker, U. Ruth, J. P. Steffensen, and V. Maggi (2008), Dust-climate couplings over the past 800,000 years from the EPICA Dome C ice core, *Nature*, *452*, 616–619, doi:10.1038/nature06763.
Lambert, F., A. Tagliabue, G. Shaffer, F. Lamy, G. Winckler, L. Farias, L. Gallardo, and R. De Pol-Holz (2015), Dust fluxes and iron fertilization in Holocene and Last Glacial Maximum climates, *Geophys. Res. Lett.*, *42*, 6014–6023, doi:10.1002/2015GL064250.
Lamy, F., R. Gersonde, G. Winckler, O. Esper, A. Jaeschke, G. Kuhn, J. Ullermann, A. Martínez-García, F. Lambert, and R. Kilian (2014), Increased dust deposition in the Pacific Southern Ocean during glacial periods, *Science*, *343*(6169), 403–407, doi:10.1126/science.1245424.
Lannuzel, D., V. Schoemann, J. de Jong, J. L. Tison, and L. Chou (2007), Distribution and biogeochemical behavior of iron in the East Antarctic sea ice, *Mar. Chem.*, *106*, 18–32, doi:10.1016/j.marchem.2006.06.010.
Li, G., and S.-P. Xie (2014), Tropical biases in CMIP5 multimodel ensemble: The excessive equatorial Pacific cold tongue and double ITCZ problems, *J. Clim.*, *27*, 1765–1780, doi:10.1175/JCLI-D-13-00337.1.
Lunt, D., and P. Valdes (2002), Dust deposition and provenance at the Last Glacial Maximum and present day, *Geophys. Res. Lett.*, *29*(22), 2085, doi:10.1029/2002GL015656.
Luo, C., N. Mahowald, T. Bond, P. Y. Chuang, P. Artaxo, R. Siefert, Y. Chen, and J. Schauer (2008), Combustion iron distribution and deposition, *Global Biogeochem. Cycles*, *22*, GB1012, doi:10.1029/2007GB002964.
Maher, B. A., J. M. Prospero, D. Mackie, D. Gaiero, P. P. Hesse, and Y. Balkanski (2010), Global connections between aeolian dust, climate and ocean biogeochemistry at the present day and at the Last Glacial Maximum, *Earth Sci. Rev.*, *99*, 61–97, doi:10.1016/j.earscirev.2009.12.001.
Mahowald, N. M., D. R. Muhs, S. Levis, P. J. Rasch, M. Yoshioka, C. S. Zender, and C. Luo (2006), Change in atmospheric mineral aerosols in response to climate: Last glacial period, preindustrial, modern, and doubled carbon dioxide climates, *J. Geophys. Res.*, *111*, D10202, doi:10.1029/2005JD006653.
Mahowald, N. M., et al. (2009), Atmospheric iron deposition: Global distribution, variability, and human perturbations, *Annu. Rev. Mar. Sci.*, *1*, 245–278, doi:10.1146/annurev.marine.010908.163727.
Mahowald, N. M., S. Albani, S. Engelstaedter, G. Winckler, and M. Goman (2011), Model insight into glacial-interglacial paleodust records, *Quat. Sci. Rev.*, *30*(7-8), 832–854, doi:10.1016/j.quascirev.2010.09.007.
Mahowald, N., S. Albani, J. F. Kok, S. Engelstaedter, R. Scanza, D. S. Ward, and M. G. Flanner (2014), The size distribution of desert dust aerosols and its impact on the Earth system, *Aeolian Res.*, *15*, 53–71, doi:10.1016/j.aeolia.2013.09.002.
Marticorena, B., and G. Bergametti (1995), Modeling the atmospheric dust cycle: 1. Design of a soil-derived dust emission scheme, *J. Geophys. Res.*, *100*(D8), 16,415–16,430, doi:10.1029/95JD00690.
Martin, J. H., R. M. Gordon, and S. E. Fitzwater (1990), Iron in Antarctic waters, *Nature*, *353*(6340), 156–158, doi:10.1038/345156a0.
Martínez-García, A., A. Rosell-Melé, W. Geibert, R. Gersonde, P. Masqué, V. Gaspari, and C. Barbante (2009), Links between iron supply, marine productivity, sea surface temperature, and CO_2 over the last 1.1 Ma, *Paleoceanography*, *24*, PA1207, doi:10.1029/2008PA001657.
Martínez-García, A., D. M. Sigman, H. Ren, R. F. Anderson, M. Straub, D. A. Hodell, S. L. Jaccard, T. I. Eglinton, and G. H. Haug (2014), Iron fertilization of the Subantarctic Ocean during the Last Ice Age, *Science*, *343*(6177), 1347–1350, doi:10.1126/science.1246848.
Mayewski, P. A., L. D. Meeker, M. S. Twickler, S. Whitlow, Q. Yang, W. B. Lyons, and M. Prentice (1997), Major features and forcing of high-latitude northern hemisphere atmospheric circulation using a 110,000-year-long glaciochemical series, *J. Geophys. Res.*, *102*, 26,345–26,366, doi:10.1029/96JC03365.
McGee, D., F. Marcantonio, and J. Lynch-Stieglitz (2007), Deglacial changes in dust flux in the eastern equatorial Pacific, *Earth Planet. Sci. Lett.*, *257*, 215–230, doi:10.1016/j.epsl.2007.02.033.
McGee, D., P. B. deMenocal, G. Winckler, J. B. W. Stuut, and L. I. Bradtmiller (2013), The magnitude, timing and abruptness of changes in North African dust deposition over the last 20,000 yr, *Earth Planet. Sci. Lett.*, *371–372*, 163–176, doi:10.1016/j.epsl.2013.03.054.
Meskhidze, N., W. Chameides, and A. Nenes (2005), Dust and pollution: A recipe for enhanced ocean fertilization?, *J. Geophys. Res.*, *110*, D03301, doi:10.1029/2004JD005082.
Miller, R., and I. Tegen (1998), Climate response to soil dust aerosols, *Bull. Am. Meteorol. Soc.*, *11*, 3247–3267, doi:10.1175/1520-0442(1998)011<3247:CRTSDA>2.0.CO;2.
Moore, C. M., et al. (2013), Processes and patterns of oceanic nutrient limitation, *Nat. Geosci.*, *6*, 701–710, doi:10.1038/ngeo1765.
Moore, J. K., and O. Braucher (2008), Sedimentary and mineral dust sources of dissolved iron to the world ocean, *Biogeosciences*, *5*, 631–656, doi:10.5194/bg-5-631-2008.
Moore, J. K., S. C. Doney, K. Lindsay, and N. Mahowald (2006), Nitrogen fixation amplifies the ocean biogeochemical response to decadal timescale variations in mineral dust deposition, *Tellus B*, *58*, 560–572, doi:10.1111/j.1600-0889.2006.00209.x.
Murphy, L. N., A. C. Clement, S. Albani, N. M. Mahowald, P. Swart, and M. M. Arienzo (2014), Simulated changes in atmospheric dust in response to a Heinrich stadial, *Paleoceanography*, *29*, 30–43, doi:10.1002/2013PA002550.
Okin, G., N. Mahowald, O. Chadwick, and P. Artaxo (2004), The impact of desert dust on the biogeochemistry of phosphorus in terrestrial ecosystems, *Global Biogeochem. Cycles*, *18*, GB2005, doi:10.1029/2003GB002145.
Prospero, J. M., P. Ginoux, O. Torres, S. E. Nicholson, and T. E. Gill (2002), Environmental characterization of global sources of atmospheric soil dust identified with the Nimbus 7 Total Ozone Mapping Spectrometer (TOMS) absorbing aerosol product, *Rev. Geophys.*, *40*(1), 1002, doi:10.1029/2000RG000095.
Raiswell, R., et al. (2016), Potentially bioavailable iron delivery by iceberg-hosted sediments and atmospheric dust to the Polar Ocean, *Biogeosci. Discuss.*, doi:10.5194/bg-2016-20.
Ratmeyer, V., G. Fischer, and G. Wefer (1999), Lithogenic particle fluxes and grain size distributions in the deep ocean off NW Africa: Implications for seasonal changes of aeolian dust input and downward transport, *Deep Sea Res., Part I*, *46*, 1289–1337, doi:10.1016/S0967-0637(99)00008-4.
Scanza, R. A., N. Mahowald, S. Ghan, C. S. Zender, J. F. Kok, X. Liu, Y. Zhang, and S. Albani (2015), Modeling dust as component minerals in the Community Atmosphere Model: Development of framework and impact on radiative forcing, *Atmos. Chem. Phys.*, *15*, 537–561, doi:10.5194/acp-15-537-2015.
Schroth, A. W., J. Crusius, E. R. Sholkovitz, and B. C. Bostick (2009), Iron solubility driven by speciation in dust sources to the ocean, *Nat. Geosci.*, *2*, 337–340, doi:10.1038/ngeo501.
Serno, S., G. Winckler, R. F. Anderson, E. Maier, H. Ren, R. Gersonde, and G. H. Haug (2015), Comparing dust flux records from the Subarctic North Pacific and Greenland: Implications for atmospheric transport to Greenland and for the application of dust as a chronostratigraphic tool, *Paleoceanography*, *30*, 583–600, doi:10.1002/2014PA002748.
Shao, Y., K.-H. Wyrwoll, A. Chappell, J. Huang, Z. Lin, G. H. McTainsh, M. Mikami, T. Y. Tanaka, X. Wang, and S. Yoon (2011), Dust cycle: An emerging core theme in Earth system science, *Aeolian Res.*, *2*, 181–204.
Shi, Z., M. D. Krom, T. D. Jickells, S. Bonneville, K. S. Carslaw, N. Mihalopoulos, A. R. Baker, and L. G. Benning (2012), Impacts on iron solubility in the mineral dust by processes in the source region and the atmosphere: A review, *Aeolian Res.*, *5*, 21–42, doi:10.1016/j.aeolia.2012.03.001.

Sholkovitz, E., P. Sedwick, T. Church, A. Baker, and C. Powell (2012), Fractional solubility of aerosol iron: Synthesis of a global-scale data set, *Geochim. Cosmochim. Acta*, *89*, 173–189, doi:10.1016/j.gca.2012.04.022.

Sudarchikova, N., U. Mikolajewicz, C. Timmreck, D. O'Donnell, G. Schurgers, D. Sein, and K. Zhang (2015), Modelling of mineral dust for interglacial and glacial climate conditions with a focus on Antarctica, *Clim. Past*, *11*, 765–779, doi:10.5194/cp-11-765-2015.

Tagliabue, A., L. Bopp, and O. Aumont (2009), Evaluating the importance of atmospheric and sedimentary iron sources to Southern Ocean biogeochemistry, *Geophys. Res. Lett.*, *36*, L13601, doi:10.1029/2009GL038914.

Tagliabue, A., O. Aumont, and L. Bopp (2014), The impact of different external sources of iron on the global carbon cycle, *Geophys. Res. Lett.*, *41*, 920–926, doi:10.1002/2013GL059059.

Takemura, T., M. Egashira, K. Matsuzawa, H. Ichijo, R. O'ishi, and A. Abe-Ouchi (2009), A simulation of the global distribution and radiative forcing of soil dust aerosols at the Last Glacial Maximum, *Atmos. Chem. Phys.*, *9*, 3061–3073, doi:10.5194/acp-9-3061-2009.

Wang, S., D. Bailey, K. Lindsay, J. K. Moore, and M. Holland (2014), Impact of sea ice on the marine iron cycle and phytoplankton productivity, *Biogeosciences*, *11*, 4713–4731, doi:10.5194/bg-11-4713-2014.

Ward, D. S., S. Kloster, N. M. Mahowald, B. M. Rogers, J. T. Randerson, and P. G. Hess (2012), The changing radiative forcing of fires: Global model estimates for past, present and future, *Atmos. Chem. Phys.*, *12*(22), 10,857–10,886, doi:10.5194/acp-12-10857-2012.

Watson, A. J., D. C. E. Bakker, A. J. Ridgwell, P. W. Boyd, and C. S. Law (2000), Effect of iron supply on Southern Ocean CO_2 uptake and implications for glacial atmospheric CO_2, *Nature*, *407*, 730–733, doi:10.1038/35037561.

Werner, M., I. Tegen, S. P. Harrison, K. E. Kohfeld, I. C. Prentice, Y. Balkanski, H. Rodhe, and C. Roelandt (2002), Seasonal and interannual variability of the mineral dust cycle under present and glacial climate conditions, *J. Geophys. Res.*, *107*(D24), 4744, doi:10.1029/2002JD002365.

Winckler, G., R. F. Anderson, M. Q. Fleisher, D. McGee, and N. Mahowald (2008), Covariant glacial-interglacial dust fluxes in the equatorial Pacific and Antarctica, *Science*, *320*, 93–96, doi:10.1126/science.1150595.

Yue, X., H. Wang, H. Liao, and D. Jiang (2011), Simulation of the direct radiative effect of mineral dust aerosol on the climate at the Last Glacial Maximum, *J. Clim.*, *24*, 843–858, doi:10.1175/2010JCLI3827.1.

Zender, C. S., H. Bian, and D. Newman (2003), Mineral dust entrainment and deposition (DEAD) model: Description and 1990s dust climatology, *J. Geophys. Res.*, *108*(D14), 4416, doi:10.1029/2002JD002775.

Zhu, X., J. Prospero, and F. Millero (1997), Diel variability of soluble Fe(II) and soluble total Fe in North Africa dust in the trade winds at Barbados, *J. Geophys. Res.*, *102*, 21,297–21,305, doi:10.1029/97JD01313.

Ziegler, M., P. Diz, I. R. Hall, and R. Zahn (2013), Millennial-scale changes in atmospheric CO_2 levels linked to the Southern Ocean carbon isotope gradient and dust flux, *Nat. Geosci.*, *6*, 457–461, doi:10.1038/ngeo1782.